9-2013

Assessment Of Density Functional Theory For Describing The Correlation Effects On The Ground And Excited State Potential Energy Surfaces Of A Retinal Chromophore Model

Miquel Huix-Rotllant

Michael Filatov

Samer Gozem

Igor Schapiro

Massimo Olivucci
Bowling Green State University, molivuc@bgsu.edu

See next page for additional authors

JCTC Journal of Chemical Theory and Computation

Article

pubs.acs.org/JCTC

Assessment of Density Functional Theory for Describing the Correlation Effects on the Ground and Excited State Potential Energy Surfaces of a Retinal Chromophore Model

Miquel Huix-Rotllant,*[,†] Michael Filatov,*[,‡] Samer Gozem,[§] Igor Schapiro,[§,∥] Massimo Olivucci,*[,⊥,§] and Nicolas Ferré*[,†]

[†]Aix-Marseille Université, CNRS, Institut de Chimie Radicalaire, 13397 Marseille Cedex 20, France

[‡]Institut für Physicalische und Theoretische Chemie, Universität Bonn, Beringstr. 4, 53115 Bonn, Germany

[§]Department of Chemistry, Bowling Green State University, Bowling Green, Ohio 43402, United States

[∥]Max Planck Institute for Chemical Energy Conversion, Stiftstr. 34 - 36, Mülheim an der Ruhr, Germany

[⊥]Dipartimento di Chimica, Università di Siena, Siena, Italy

Supporting Information

ABSTRACT: In the quest for a cost-effective level of theory able to describe a large portion of the ground and excited potential energy surfaces of large chromophores, promising approaches are rooted in various approximations to the exact density functional theory (DFT). In the present work, we investigate how generalized Kohn−Sham DFT (GKS-DFT), time-dependent DFT (TDDFT), and spin-restricted ensemble-DFT (REKS) methods perform along three important paths characterizing a model retinal chromophore (the penta-2,4-dieniminium cation) in a region of near-degeneracy (close to a conical intersection) with respect to reference high-level multiconfigurational wave function methods. If GKS-DFT correctly describes the closed-shell charge transfer state, only TDDFT and REKS approaches give access to the open-shell diradical, one which sometimes corresponds to the electronic ground state. It is demonstrated that the main drawback of the usual DFT-based methods lies in the absence of interactions between the charge transfer and the diradicaloid configurations. Hence, we test a new computational scheme based on the State-averaged REKS (SA-REKS) approach, which explicitly includes these interactions into account. The State-Interaction SA-REKS (SI-SA-REKS) method significantly improves on the REKS and the SA-REKS results for the target system. The similarities and differences between DFT and wave function-based approaches are analyzed according to (1) the active space dimensions of the wave function-based methods and (2) the relative electronegativities of the allyl and protonated Schiff base moieties.

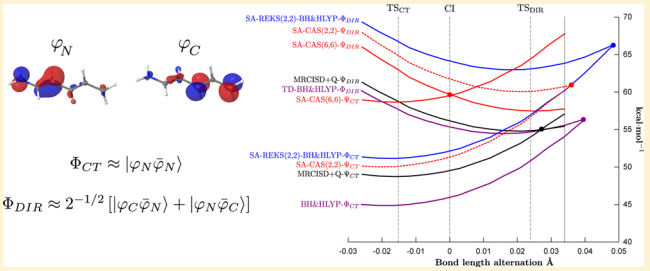

1. INTRODUCTION

The penta-2,4-dieniminium cation (PSB3), a protonated imine featuring three conjugated double bonds (see Scheme 1), is currently one of the most popular computational models of the retinal chromophore found in visual pigments. Its electronic structure has been recently studied using various levels of *ab initio* multireference theory.[1] In the vicinity of a conical intersection (CI), which is characterized by a ca. 90°-twisted C_2-C_3 bond, the electronic structure of PSB3 has been analyzed along a loop spanned by the branching space vectors. It was found that a covalent/diradicaloid electronic structure (Ψ_{DIR}), which leads to the homolytic dissociation of PSB3 central double bond, characterizes a large region on the ground state (S_0) potential energy surface (PES). The rest of the S_0 PES, the extent of which depends on the selected level of theory, is characterized by a shifted positive charge from the Schiff base ($N^+-C_1-C_2$) to the allyl fragment ($C_3-C_4-C_5$) and a wave function (Ψ_{CT}) with a dominating charge transfer character similar to the first singlet excited electronic state in the Franck−Condon region. Each of the two regions features a unique transition state connecting the 2-*cis* and 2-*trans* conformations of PSB3, which will be denoted TS_{CT} and TS_{DIR}.

Scheme 1. Numbering Scheme for Penta-2,4-dieniminium Cation

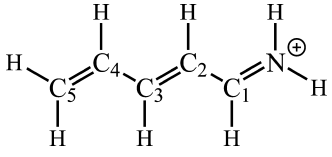

The correct description of the PES around the CI requires an accurate and balanced account of dynamic and nondynamic

Received: April 29, 2013
Published: August 13, 2013

   dx.doi.org/10.1021/ct4003465 | *J. Chem. Theory Comput.* 2013, 9, 3917−3932

correlation effects. Recently, a series of multiconfigurational wave function methods ranging from the complete active space self-consistent field (CASSCF) method to post-CASSCF correlated methods have been used to calculate the S_0 electronic structure along three pathways constructed on the PES from CASSCF calculations.[1] The first pathway connects TS_{DIR} and TS_{CT} and intercepts the CI. This pathway is characterized by varying the bond length alternation (BLA) coordinate, which is defined as the difference between the average length of formally single bonds and the average length of formally double bonds in PSB3.[1] This coordinate approximately follows the unscaled gradient difference vector.[1] The remaining two pathways are constructed as the minimum energy pathways (MEPs) connecting the reactant (*2-cis*-PSB3) to the product (*2-trans*-PSB3), however, intercepting either TS_{DIR} (MEP_{DIR}) or TS_{CT} (MEP_{CT}). These MEPs correspond to a movement that twists the central C_2-C_3 double bond and, near the 90° of twist, are aligned with the direction of the interstate coupling vector.[1]

The results of multireference calculations carried out by Gozem et al.[1] show that the inclusion of the dynamic electron correlation can radically change the topology of the region surrounding the CI, thus offering a good test for other correlated methods. More recently, a series of the spin-flip (SF) equations-of-motion (EOM) coupled-cluster methods have been applied to study the ground and the excited state PES profiles along the three MEPs in the PSB3 retinal model.[2] In particular, it was found that the SF-EOM-CCSD(dT) method based on the spin-restricted open-shell Hartree−Fock (ROHF) triplet reference state provides an excellent agreement with the MRCISD+Q results. The spin-flip excitations included into the SF-EOM-CCSD approach account for the multireference character of the ground and excited states of the PSB3 model. However, the steep scaling of the computational time with the system size precludes the application of the EOM-CCSD(dT) approach to large molecular systems.

In the present paper, we evaluate the performance of a series of computationally efficient electronic structure methods rooted in density functional theory (DFT) in the calculation of the PSB3 PESs near the CI region obtained at the CASSCF level of theory. DFT is a formally exact theory, although in practice one has to approximate the unknown exchange-correlation (XC) functional which accounts for all the many-body effects. Due to their low computational cost, these methods can be easily applied to the full retinal molecule or used for on-the-fly quantum chemical calculations in molecular dynamics simulations.

In the following, we report the results obtained using DFT-based computational schemes in the calculation of the three pathways investigated in ref 1 which correspond to the strongly correlated region on the PSB3 ground and excited state PESs and the vicinity of the CI. Note that we are not concerned with the determination of real conical intersections but mainly with the quality of the description of the electron correlation captured by the selected methods. The corresponding energy profiles and parameters of the electronic structure are compared to the CASSCF and MRCISD+Q ones, the latter being the most accurate theoretical method applied for the PSB3 retinal model.

2. THEORETICAL REMARKS

The success of Kohn−Sham DFT (KS-DFT)[3] is attributed to the inclusion of electron correlation at a low computational cost via the use of approximations to the exact XC functional. The existing approximations to the XC functional of KS-DFT focus primarily on the dynamic electron correlation, such as that encountered in rare gas atoms.[4] Although the current semilocal XC functionals also provide for a certain nonspecific account of nondynamic correlation,[5] the treatment of strongly correlated electronic systems still remains problematic and may require to go beyond the conventional paradigm of KS-DFT.

KS-DFT is based on the notion that the ground state density of a real many-electron system can be uniquely mapped on the ground state density of a fictitious system of noninteracting particles moving in a suitably modified external potential.[3] The possibility to represent the target density by a single KS determinant built from the lowest eigenfunctions of a non-interacting system is known as the pure-state v-representability (PS-VR). CI regions are an example where PS-VR typically fails and therefore are problematic for most widely used DFT methods based on the KS approach. Indeed, topological nonanalyticities in the density have been shown to occur in the CI seam by R. Baer.[6] Twisting about the double bond in ethene clearly illustrates the PS-VR problem.[7] When the molecule is 90° twisted, there is a degeneracy of the π and π^* molecular orbitals, and the single-reference KS *Ansatz* breaks down. The same occurs with a twisted PSB3 in the region of the PES close to the CI. The choice of an approximate functional can modulate where the orbital degeneracy occurs; however, irrespective of the density functional employed, it is not possible to correctly describe the ground state PES at all points. Another consequence of the lack of genuine multireference character in KS-DFT is that the ground and the excited states do not interact. Consequently, the degeneracy obtained using KS-DFT is lifted along one degree of freedom only, resulting in an intersection space of wrong dimensionality ($3N - 7$ instead of $3N - 8$), as in the case of ethene[7] and similarly observed in the present study.

At variance with ethene, PSB3 comprises two different moieties with respect to the central chemical bond, a protonated Schiff base and an allyl group featuring different electronegativities, which break the exact degeneracy of the π and π^* orbitals near the S_0/S_1 CI space. In this region, the minimal active space comprises two electrons in two orbitals (Figure 1), denoted by φ_N for the Schiff base part and φ_C (localized on the allyl part). Two singlet electronic configurations are important to represent the crossing between the states. The $\Phi_{DIR} = 2^{-1/2}(|\varphi_C\bar{\varphi}_N\rangle + |\varphi_N\bar{\varphi}_C\rangle)$ configuration shows a diradicaloid

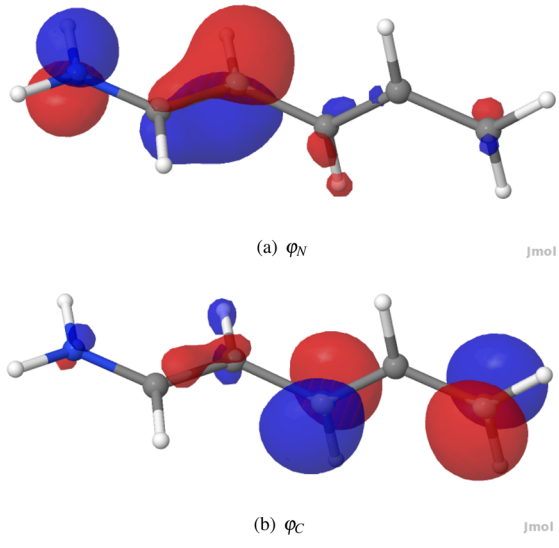

Figure 1. Kohn−Sham frontier orbitals (B3LYP/6-31G(d)).

dx.doi.org/10.1021/ct4003465 | *J. Chem. Theory Comput.* 2013, 9, 3917−3932

character and, at the multireference wave function theory level, represents the major contribution to the Ψ_{DIR} wave function near the CI seam. The $\Phi_{CT} = |\varphi_N\bar{\varphi}_N\rangle$ configuration corresponds to a (positive) charge transfer from the N-side to the C-side (with respect to the Franck−Condon ground state charge distribution) and is the leading configuration in the Ψ_{CT} wave function. Near the CI which is near ca. 90° twisted about the C_2-C_3 double bond, S_0 changes its character from Φ_{DIR} to Φ_{CT} (or back) when moving along the BLA coordinate.

KS-DFT can only describe Φ_{CT}, since Φ_{DIR} is not a single-reference state. Thus, at the geometries for which the ground state is dominated by Φ_{DIR}, KS-DFT yields the density of the excited CT state. In this case, the application of linear-response time-dependent DFT (hereafter simply denoted TDDFT) may result in an imaginary excitation energy to the lower energy diradicaloid state. It is worth noting that this imaginary excitation energy has a different origin than the one that arises from an (triplet or near singlet) instability of the restricted KS-DFT solution whenever there exists a more stable (spin) broken-symmetry solution.[8,9] In the latter case, the use of the Tamm−Dancoff approximation (TDA) largely remedies the instability; however, it has little effect in the former case as it will be seen in the present study.

Pure, hybrid, or range-separated DFT functionals have already been used to study both ground and excited states of PSB3 or other models of retinal. Tajkhorshid and Suhai studied the environment effects on the structure of several retinal models using the BLYP functional.[10,11] In the context of plane-wave molecular dynamics simulations of retinal inside the rhodopsin protein, Röthlisberger and co-workers have employed the restricted open-shell Kohn−Sham (ROKS) method.[12] However, the pure GGA functional used in these works does not correctly describe the parts of the ground and excited state PESs with which we are interested in, in the present study (see below). Frauenheim, Elstner, and co-workers ran molecular dynamics simulations of large models of the retinal+protein system using the tight-binding DFT method.[13−15] The latter, however, is based on the single-reference KS-DFT description and cannot be used for strongly correlated areas of the PSB3 PES.

In 2002, Torii performed geometry optimization and vibrational analysis of retinal using the B3LYP hybrid functional.[16] Nakajima et al. investigated the protonation states of bacteriorhodopsin using an integrated linear-scaling scheme in which retinal and its close surroundings are modeled by means of the B3LYP calculations.[17] Gascon and Batista performed hybrid QM/MM calculations using the B3LYP and TD-B3LYP approaches to determine how the energy is stored when retinal absorbs a photon.[18] Touw et al.[19] complement the previous studies by molecular dynamics and static calculations using either the BP86 pure functional or the B3LYP hybrid functional. At the same time, Wanko et al.[20] and Fantacci et al.[21] simultaneously published the first critical analyzes of the capability of TDDFT to describe excited states of retinal models (including PSB3). While vertical excitation energies from the TD-BP86 and TD-B3LYP calculations are sufficiently accurate, as compared to experiment or high level *ab initio* results, the energy gradient for the Franck−Condon geometry points in the wrong direction, enlarging the bond length alternation. The same observations have been made by Aquino et al.[22]

Despite the warnings issued in these articles, the PESs of retinal models were still investigated by TDDFT using the same functionals. Send and Sundholm ran TDDFT calculations to study the full retinal molecule, again with the B3LYP functional,[23,24] while others restrict their use to ground state geometries and excitation energies.[25] It is noteworthy that a qualitative agreement is often found with the energies and excited state structures computed at the *ab initio* CC2 level.[23,24] Because the description of charge-transfer excited states is known to be problematic for standard hybrid functionals, new range-separated functionals were devised and applied to retinal models. In 2006, Hirao and co-workers proposed long-range corrections to several DFT pure or hybrid functionals.[26] First excited state geometries and excitation energies obtained with the LC-BOP functional were closer to CASPT2 ones than those obtained with the usual B3LYP functional. In the same spirit, other authors have used the CAM-B3LYP functional and found a significant improvement for both ground and excited state properties of retinal.[27,28] Recently, Valsson and Filippi have suggested that M06-2X would give better ground state structures.[29,30]

In the present study, we test the ability of different flavors of DFT functionals to deal with the PSB3 electronic structure around the CI seam. This CI is in a region where the noninteracting v-representability of KS-DFT breaks down. When using pure density functionals, this manifests itself in the lack of convergence of the self-consistent KS procedure due to the vanishing HOMO−LUMO gap. The inclusion of a portion of the Hartree−Fock exchange in hybrid, range-separated hybrid and double hybrid functionals may improve the SCF convergence away from the CI region; however, the convergence problems still persist near the CI seam. We would like to make the reader aware that the use of some portion of Hartree−Fock exchange is possible only by generalizing the classic Kohn−Sham equations to accept nonlocal potentials.[31] For the sake of readability, we keep hereafter the KS acronym. The selection of functionals employed in the present work comprises two hybrid functionals (B3LYP, BH&HLYP), a hybrid meta-GGA functional (M06-2X), a range-separated hybrid (CAM-B3LYP), and double-hybrid (mPW2PLYP) functional, which span four rungs of the Jacob's ladder of DFT.[32]

Theoretical approaches beyond KS-DFT accounting for static correlation more accurately can potentially improve the quality of description of the PSB3 electronic structure. Spin-flip TDDFT (SF-TDDFT)[33] is one of such methods. It relies on a triplet reference state, in most cases correctly represented by the standard KS-DFT, and uses the spin-flip *Ansatz* to reach singlet ground and excited states. The main advantage of SF-TDDFT is that it may accommodate some multireference character of the singlet ground electronic state via inclusion of the singlet doubly excited electronic configuration. Unfortunately, all our attempts to apply SF-TDDFT to PSB3 have been unsuccessful, mainly due to the spin-contamination that neither a restricted description of the reference triplet state nor the use of a noncollinear XC kernel helped to overcome. Even though spin-correction techniques may be applied to correct *a posteriori* this spin-contamination problem as shown by Xu et al.,[34] we focus on alternative approaches in the present study.

Ensemble DFT represents a promising route to ameliorate the shortcomings of the conventional KS-DFT for the description of nondynamic electron correlation, where going beyond the PS-VR restriction might be required. It was theoretically demonstrated already in the early days of DFT that some physical densities cannot be obtained by a noninteracting pure state potential. In the works of Lieb,[35] H. Englisch and R. Englisch,[36] and Kohn and co-workers,[37] it has been demonstrated that many non-PS-VR physical densities are non-interacting ensemble v-representable (E-VR). E-VR implies

dx.doi.org/10.1021/ct4003465 | J. Chem. Theory Comput. 2013, 9, 3917−3932

that the density is represented by a weighted sum (ensemble) of densities of several KS determinants, which results in the fractional occupation numbers (FONs) of the KS orbitals. The works of Baerends and co-workers[38] and Morrison[39] have demonstrated that ensemble representation of the density is not merely a theoretical curiosity but may be practically applied to DFT. Using the first principles approach based on the search for a KS potential for the known exact density (density from high-level *ab initio* calculations), it has been shown that one needs to switch to the ensemble representation for the density of a noninteracting reference system in the cases where the strong nondynamic correlation is present in the interacting (physical) limit.

The early attempts to employ the ensemble representation have led to the realization that density functionals of KS-DFT have to be specifically adapted to accommodate the ensemble densities, or equivalently, the FONs of KS orbitals.[40] A successful construction of a generally applicable representation for the XC functional in ensemble DFT has been achieved in the spin-restricted ensemble-referenced KS (REKS) method.[41] The REKS method is based on a rigorous statement by Lieb[35] that, for any physical density represented by an ensemble of KS states, the energy can be represented by an ensemble of the energies of the individual states using the same weighting factors. The derivation of ensemble representations for the density and the energy, and the derivation of relationships between the ensemble weighting factors and the FONs of the REKS orbitals, was guided by the analysis of a number of model multireference problems at the wave function theory level.[41−43] In this way, the REKS method inherits the nomenclature developed for the multi-reference wave function methods. Thus, in the REKS(2,2) (two active electrons in two active space orbitals) method, the occupied KS orbitals are split in two subsets, a subset of the doubly occupied core orbitals and a subset of two fractionally occupied active space orbitals, the FONs of which are variationally optimized together with the core and active REKS orbitals.[41] While the REKS method is capable of accurately describing the strongly correlated ground states of molecules, the state-averaged REKS (SA-REKS) method[44] gives access to the lowest singlet excited state of a molecular system typified by the strong nondynamic electron correlation in the ground state, such as ethene near 90° of twist or PSB3 near the CI. In this regard, the REKS and the SA-REKS methods are very well suited for the description of the states involved in the photoisomerization of PSB3 (and retinal).

3. COMPUTATIONAL DETAILS

Details about optimization of the geometries used in this study are given in ref 1. In short, they have been obtained at CASSCF level of theory with two roots equally averaged (denoted SA-CAS(6,6) in the following), whose active space includes 6 electrons in 6 π-type orbitals. The 6-31G(d) basis set was used in the previous studies[1,2] and is also used in the present one. SA-CAS(6,6) and MRCISD+Q energies are taken from ref 1, while SF-EOMCC ones are obtained from ref 2. For analysis purposes, we also carried out the same kind of calculations based on a smaller active space (2 electrons in 2 orbitals). The corresponding calculations have been performed using the Molcas 7 package.[45]

TDDFT Calculations. The TDDFT equations are solved within the linear response approach. The full response TDDFT equations are given by

$$\begin{bmatrix} A & B \\ -B^* & -A^* \end{bmatrix}\begin{bmatrix} X \\ Y \end{bmatrix} = \omega\begin{bmatrix} X \\ Y \end{bmatrix} \tag{1}$$

where the matrices **A** and **B** are defined as

$$A_{ai,bj} = \delta_{ab}\delta_{ij}(\varepsilon_a - \varepsilon_i) + (ia|f_{\mathrm{Hxc}}|bj) \tag{2}$$

$$B_{ai,bj} = (ia|f_{\mathrm{Hxc}}|jb) \tag{3}$$

The indexes *a,b,...* and *i, j,...* indicate virtual and occupied spin−orbital indexes respectively, the ε_p are KS orbital energies, and f_{Hxc} is the Hartree-exchange-correlation kernel in the adiabatic approximation,

$$f_{\mathrm{Hxc}}(r, r') = \frac{1}{|r - r'|} + \frac{\delta^2 E_{\mathrm{xc}}[\rho]}{\delta\rho(r)\delta\rho(r')} \tag{4}$$

The TDA to the full response equations consists in setting $\mathbf{B} = \mathbf{0}$, thus solving the TDDFT(TDA) equation

$$\mathrm{AX} = \omega\mathrm{X} \tag{5}$$

with the same definition of the **A** as for the full response equations. The TDA approximation decouples the ground- and the excited-states and can improve the results when the ground-state is not well described. The TDA approximation is shown to improve both singlet→triplet and singlet→singlet excitation energies.[9]

The full response TDDFT equations have been performed with Gaussian09.[46] All TDDFT(TDA) calculations have been carried out with GAMESS-US,[47,48] apart from calculations with mPW2PLYP functionals, which have employed the Orca package.[49]

REKS and SA-REKS Calculations. The working equations of the REKS method have been derived on the basis of rigorous theoretical results concerning representation of the exact physical density and the energy functional via ensembles (weighted sums) of several PS-VR KS states (cf. Theorems 4.2 and 4.3 and eqs (4.5) and (4.7) in refs 35 and 38). Thus, the energy and the density of a strongly correlated electronic state are represented in the REKS method by weighted sums of the energies and densities of several electronic configurations represented by the respective KS determinants built on the same set of the KS orbitals.[41,43]

Using this representation, the REKS(2,2) total density and energy are given by eqs 6 and 7,

$$\rho^{\mathrm{REKS}(2,2)}(r) = \sum_{k}^{\mathrm{core}} 2|\varphi_k(r)|^2 + n_a|\varphi_a(r)|^2 + n_b|\varphi_b(r)|^2 \tag{6}$$

$$E^{\mathrm{REKS}(2,2)} = \frac{n_a}{2}E[...\varphi_a\bar{\varphi}_a] + \frac{n_b}{2}E[...\varphi_b\bar{\varphi}_b] + f(n_a, n_b)E[...\varphi_a\varphi_b] - \frac{f(n_a, n_b)}{2}E[...\varphi_a\bar{\varphi}_b] - \frac{f(n_a, n_b)}{2}E[...\bar{\varphi}_a\varphi_b] \tag{7}$$

where φ_k are the doubly occupied core orbitals, φ_a and φ_b are the fractionally occupied active orbitals with the occupation numbers n_a and n_b, respectively, $f(n_a,n_b)$ is a function of the occupation numbers, and the unbarred and barred orbitals are occupied with spin-up and spin-down electrons, respectively.

The REKS density (eq 6) describes the ensemble density associated with the first two terms on the right-hand side of eq 7

whereas the KS densities of the last three terms in eq 7 sum up to zero. Although the latter three KS states yield zero contribution to the density, their contribution to the energy is nonvanishing and it amounts to a DFT analogue of the exchange integral between the fractionally occupied (active) orbitals. The occurrence of such a term in the energy expression can be illustrated by the following argument (see ref 41 for more details). At a completely noninteracting KS limit, the KS density with two fractionally occupied KS orbitals can be described by an ensemble of two KS single determinant configurations represented by the first two terms on the right-hand side of eq 7. Let us gradually switch on the electron−electron interaction along the adiabatic connection path. Provided that the interaction remains infinitesimally weak it should not affect the wave functions and the energies of all but two electrons, namely the two electrons in the fractionally occupied (and therefore degenerate) KS orbitals.[38,50] For such a case, the application of quasi-degenerate perturbation theory to obtain the total energy of the system leads to eq 7, in which $f(n_a,n_b) = (n_a,n_b)^{1/2}$.

The actual algebraic form of the function $f(n_a,n_b)$ is obtained from interpolating between the limits of an ensemble KS state (see above) and a single-reference KS state.[43] This is done to eliminate the double counting of the nondynamic electron correlation and to guarantee that, for a state which is correctly described by a single KS determinant, the REKS method yields the same energy as the standard single-reference KS-DFT.[41,43] Details of the derivation can be found in previous works on the REKS methodology, see refs 41 and 43.

The REKS(2,2) energy is minimized with respect to the orbitals and the fractional occupation numbers of the active orbitals under the constraint of orbital orthonormality and the constraint for active orbital occupation numbers $n_a + n_b = 2$.[41] The orbital orthogonality constraint is imposed by the use of the method of Lagrange multipliers, which leads to the well-known general open-shell self-consistent field equations.[51] Note that, because the REKS energy functional is explicitly dependent on the fractional occupation numbers of the active orbitals which preserve the correct number of particles,[41] there is no need to impose the occupation number constraint and the REKS functional is optimized with respect to n_a and n_b directly without resorting to the use of Lagrange multipliers. However, as the REKS energy (eq 7) is stationary with respect to the fractional occupation numbers of the active orbitals, the respective Lagrange multipliers, if they were obtained, would become strictly degenerate, see ref 50 for more detail. Further details of the REKS methodology can be found in refs 41 and 43. The outlined REKS method can be used in connection with any approximate local or semilocal density functional.

The REKS(2,2) method describes a diradicaloid state, for which the noninteracting KS reference wave function is given by

$$\Phi_0 = \sqrt{\frac{n_a}{2}}|...\varphi_a\bar{\varphi}_a\rangle - \sqrt{\frac{n_b}{2}}|...\varphi_b\bar{\varphi}_b\rangle \tag{8}$$

The orbitals φ_a and φ_b can be localized on specific fragments in the molecule, such as the φ_C and φ_N orbitals in Figure 1, or delocalized over the two fragments as $\varphi_a \approx \varphi_C + \varphi_N$ and $\varphi_b \approx \varphi_C - \varphi_N$.[52] In the space of two active orbitals φ_a and φ_b, excitation of a single electron from this state leads to an open-shell singlet (OSS) state:

$$\Phi_1 = \frac{1}{\sqrt{2}}|...\varphi_a\bar{\varphi}_b\rangle + \frac{1}{\sqrt{2}}|...\varphi_b\bar{\varphi}_a\rangle \tag{9}$$

which represents the lowest singlet excited state of a biradical.[52] In the localized representation of the active orbitals, that is $\varphi_a = \varphi_C$ and $\varphi_b = \varphi_N$, the latter state has a predominantly covalent character, whereas the state described by eq 8 is largely ionic. Note that the localized and delocalized representation of the active orbitals in a diradical are complementary.[52]

The energies of the two states, Φ_0 and Φ_1, can be obtained with the use of the SA-REKS method, in which a weighted sum of the energies of these states is minimized with respect to the KS orbitals and, for the Φ_0 state, their fractional occupation numbers.[44] In the SA-REKS energy functional,

$$E^{\text{SA-REKS}} = C_0E_0^{\text{REKS(2,2)}} + C_1E_1^{\text{ROKS}}, \quad C_0 + C_1 = 1 \tag{10}$$

the ground state energy is calculated using the REKS(2,2) method, and the OSS excited state energy is calculated using the ROKS method.[44,53] Typically, equal weighting factors C_0 and C_1 are chosen in practical calculations.

The OSS state (eq 9) represents the lowest excited state of a homopolar biradical,[52] such as the dissociating H_2 molecule or ethene at 90° of twist. For a heteropolar biradical, such as PSB3 near the CI, the two states, Φ_0 and Φ_1, can mix thus leading to states with partial covalent and partial ionic character.[52,54] Within the SA-REKS formalism, this mixing can be described by a simple 2×2 secular problem in the space of the two states, Φ_0 and Φ_1.[55] The diagonal elements of the Hamiltonian matrix are given by $E_0^{\text{REKS(2,2)}}$ and E_1^{ROKS}, calculated using the SA-REKS orbitals, and the off-diagonal element is given by

$$\begin{aligned} H_{12} &= n_a\sqrt{n_a}\langle\varphi_b|\hat{F}_a|\varphi_a\rangle - n_b\sqrt{n_b}\langle\varphi_a|\hat{F}_b|\varphi_b\rangle \\ &= (\sqrt{n_a} - \sqrt{n_b})W_{ab} \end{aligned} \tag{11}$$

which is obtained by the application of Slater−Condon rules and the variational condition for the REKS orbitals.[41,51,53] In eq 11, $\hat{F}_a$ and $\hat{F}_b$ are the Fock operators for the orbitals φ_a and φ_b, respectively, and W_{ab} is the off-diagonal Lagrange multiplier for the open-shell orbitals φ_a and φ_b. Provided that the equal weighting factors are chosen in SA-REKS (eq 10), the state-averaged energy functional remains unchanged upon the application of the described procedure and the SA-REKS orbitals do not need to be reoptimized. Although the correction to the $E_0^{\text{REKS(2,2)}}$ and E_1^{ROKS} energies is sufficiently small, the outlined procedure yields a more realistic description of the ground and excited states, especially when the excitation energy is very small, such as in PSB3 near the CI. In the following, this approach will be denoted as the state-interaction SA-REKS (SI-SA-REKS), for brevity.

The REKS(2,2) and SA-REKS methods are implemented in the COLOGNE2012 program,[56] which was used in the calculations. The analytic energy gradient is available for the REKS(2,2) method; however, it is not yet implemented for the individual states in the SA-REKS method. This implies that the relaxed density matrix is not yet available for the ground and the excited states in the SA-REKS approach and the electron density distribution can be obtained using the state-averaged orbitals only.

4. RESULTS

4.1. Energy Gaps and Bond Length Alternation Coordinate. The BLA path intercepts three important structures determined at the SA-CAS(6,6) level of theory (TS_{DIR}, TS_{CT}, and the CI) whose relative stabilities govern the

dx.doi.org/10.1021/ct4003465 | J. Chem. Theory Comput. 2013, 9, 3917−3932

thermal or photochemical isomerization of PSB3. The accuracy of the approximate methods selected in this work can be first tested against reference levels of theory (SA-CAS(6,6), MRCISD+Q, and SF-EOMCCSD(dT)/ROHF) for which the $S_0 \rightarrow S_1$ energy gaps, ΔE, are computed at particular geometries, namely the *cis* minimum and both TS_{CT} and TS_{DIR}. The corresponding values are reported in Table 1. As it is well-known for retinal models, the addition of dynamic electron correlation to CASSCF dramatically affects ΔE.

Table 1. $S_0 \rightarrow S_1$ Energy Gaps (ΔE, in kcal/mol) at TS_{CT}, TS_{DIR}, and *cis* PSB3[a]

method	ΔE at TS_{CT}	ΔE at TS_{DIR}	ΔE at 2-*cis*-PSB3
	References		
MRCISD+Q	10.2	0.6	101.4
SF-EOMCCSD(dT)/ROHF	11.1	0.6	102.1
SA-CAS(6,6)	4.5	7.4	110.3
	TDDFT		
B3LYP	−8.1	−3.6	98.8
B3LYP(TDA)	−7.9	−14.7	109.2
BH&HLYP	13.0	3.6	103.7
BH&HLYP(TDA)	13.3	3.9	112.1
M06-2X	5.2	−3.3	100.5
M06-2X(TDA)	5.7	−2.7	109.4
CAM-B3LYP	6.6	−1.9	101.2
CAM-B3LYP(TDA)	6.8	−1.3	110.0
mPW2PLYP(TDA)	3.1	−5.1	103.6
	SA-REKS		
HF	14.8	2.5	105.1
BH&HLYP	15.8	5.8	99.7

[a]Negative values indicate either an imaginary excitation energy or a negative one when TDA is used. They correspond to the situation where Φ_{DIR} becomes more stable than Φ_{CT} (see text).

The TDDFT ΔE values (obtained at the SA-CAS(6,6) S_0 ground state *cis* geometry) are rather insensitive to the choice of a functional. However, the use of the TDA systematically increases the energy gap at 2-*cis*-PSB3, reducing its agreement with MRCISD+Q. Interestingly, the two electrons in two orbitals SA-REKS approach, using the BH&HLYP functional or even using the Hartree−Fock functional, gives accurate ΔE values, very close to the reference.

Because the restricted KS approach is only able to find the closed shell Φ_{CT} solution, some of the TDDFT excitation energies are found to be imaginary (or negative for TDA), thus indicating that a triplet instability is present and the true ground state has a diradicaloid character as given by the Φ_{DIR} configuration. Such imaginary excitation energies are expected near the TS_{DIR} geometry. The fact that the BH&HLYP and BH&HLYP(TDA) do not show such imaginary excitations can be the result of the absence of TS_{DIR} on the S_0 potential energy surface due to the crossing topology becoming sloped rather than peaked. We recall that the geometries of the corresponding pathways have not been reoptimized. More seriously, B3LYP and B3LYP(TDA) are the only cases that result in a Φ_{DIR} ground state at both the TS_{CT} and TS_{DIR} geometries. This is due to a strong instability of the ground state, which would be partially resolved by using an unrestricted Kohn−Sham approach and the TDA approximation.[8] However, this approach is unreliable due to the strong spin contamination of the excited states. These results, along with the aforementioned gradient problem in the Franck−Condon region,[20] definitively exclude B3LYP TDDFT as a suitable method for photoisomerization studies of PSB3 and similar molecular systems. For these reasons, we exclude this functional in the rest of this work.

Examination of the SA-REKS orbital occupation numbers indicates a closed shell solution for all the three considered S_0 geometries. At the TS_{DIR} geometry, a small positive energy gap is found (5.8 kcal/mol), similar to the TDDFT result obtained using the same BH&HLYP functional. Accordingly, the choice of the functional has a large impact on the relative stability of the Φ_{DIR} and Φ_{CT} states and, consequently, on their crossing topologies.

Figure 2 displays the energy profiles obtained along the BLA path at the TDDFT level of theory, together with the reference profiles obtained previously at the SA-CAS(6,6) and MRCISD+Q levels of theory. For all the selected functionals, the Φ_{CT}

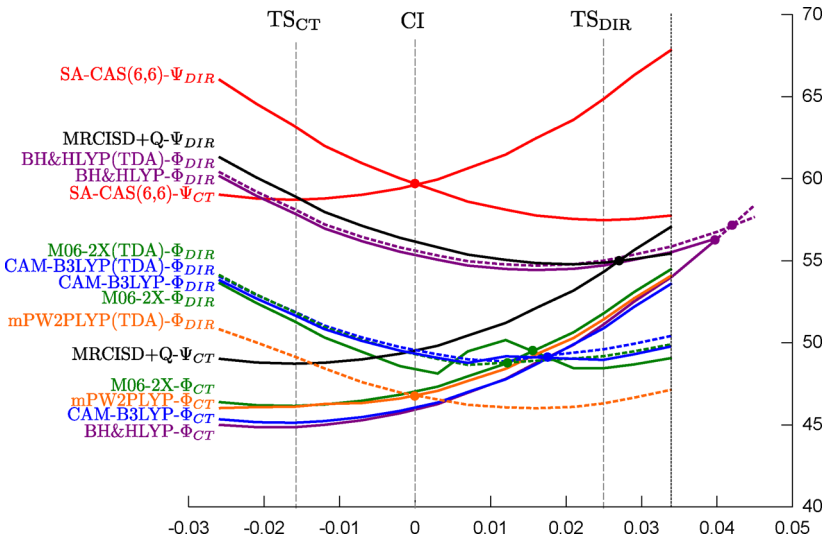

Figure 2. S_0 and S_1 energy profiles along the BLA coordinate (in Å) at different levels of theory. The energy values (in kcal/mol) are given relatively to the *cis* conformation. Crossing points are indicated with filled circles. The positions of TS_{CT}, TS_{DIR}, and the conical intersection (obtained at the SA-CAS(6,6) level of theory) are also reported. Energy profiles beyond the 0.032 coordinate value are extrapolated by a fourth-order polynomial fitting procedure.

dx.doi.org/10.1021/ct4003465 | J. Chem. Theory Comput. 2013, 9, 3917−3932

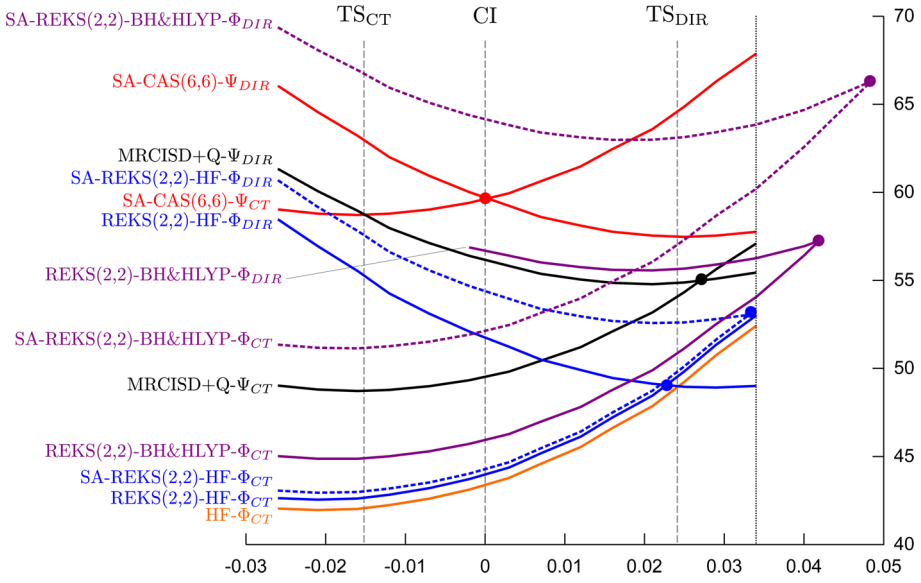

Figure 3. REKS and SA-REKS S_0 and S_1 energy profiles along the BLA coordinate (in Å). The energy values (in kcal/mol) are given relatively to the *cis* conformation. Crossing points are indicated with filled circles. The positions of TS_{CT}, TS_{DIR}, and the conical intersection (obtained at the SA-CAS(6,6) level of theory) are also reported.

profiles are smooth and continuous. Even in the region of near-degeneracy, the choice of the functional does not seem to be significant if it features a $\varphi_N - \varphi_C$ energy gap sufficiently large to provide for a good SCF convergence for Φ_{CT}. On the other hand, the calculated Φ_{DIR} profiles sometimes show discontinuities in the region between BLA values of 0.0 and 0.02. Note that BH&HLYP does not suffer from this erratic behavior; however, the corresponding Φ_{CT} and Φ_{DIR} profiles never cross in the considered BLA region. Without TDA, it can be expected that a similar erratic behavior would occur near the 0.040 BLA value. This erratic behavior of full TDDFT, already shown by Xu et al,[34] was attributed to a triplet instability which is symptomatic of a lower energy broken-symmetry ground state density. As explained above, the inability of KS-DFT to obtain the Φ_{DIR} solution is also a source of instability, as demonstrated by the imaginary excitations to the true Φ_{DIR} ground state from the Φ_{CT} excited state. The same behavior was already observed in the case of the butadiene conical intersection by Martinez and co-workers.[7] This instability cannot be simply cured by applying the TDA.

The use of TDA seems to be mandatory in order to obtain well-defined continuous curves.[34] Using this approximation, the Φ_{CT} and Φ_{DIR} energy profiles cross using CAM-B3LYP or M06-2X, between the BLA values of 0.01 and 0.02. While TDDFT(TDA) stabilizes the BH&HLYP Φ_{DIR} state, it still does not cross Φ_{CT}, the extrapolated crossing occurring at BLA slightly longer than 0.04. Nevertheless, the BH&HLYP Φ_{DIR} profile is quantitatively similar to the reference MRCISD+Q one. On the other hand, the use of the double-hybrid functional mPW2PLYP (only available with TDA) shows a crossing topology very similar to the SA-CAS(6,6) one while the crossing point energy is lower by 13 kcal/mol. Removing the perturbative part from the CIS(D) procedure[57] (i.e., the procedure that is used for obtaining the excitation energies in connection with the double hybrid density functionals[58]) does not change the crossing point coordinate, but only shifts its energy relatively to the ground state minimum (Figure S1, see the Supporting Information).

REKS and SA-REKS energy profiles, using either the Hartree−Fock or BH&HLYP functionals, are shown in Figure 3, together with the SA-CAS(6,6) and MRCISD+Q ones. In order to understand the effect of varying orbital occupation numbers, we first started from simple restricted Hartree−Fock (RHF) calculation of the ground state, Φ_{CT}. As expected, allowing the orbital occupation numbers to vary with REKS has a minor effect on the Φ_{CT} energy profile; however, this can be used to converge the Φ_{DIR} state if φ_C and φ_N orbitals are filled with one electron each at the beginning of the SCF cycles. Accordingly, a crossing between Φ_{CT} and Φ_{DIR} can be identified at BLA coordinate ~0.023. However, this procedure has the major disadvantage to require two separate calculations, with different initial guesses for the occupation numbers. Furthermore, the two states obtained in separate calculations may not represent the ground and the excited state of the same system, because the KS orbitals of the one state are not orthogonal with respect to the orbitals of the other state. Thus, an orthogonalization of the obtained states is required,[59] and the direct use of the energies obtained in separate sets of calculations, as was done in ref 34, cannot be generally recommended in the regions of the PES where electronic state degeneracies are important. This can be remedied using the SA-REKS method in which both Φ_{CT} and Φ_{DIR} states are obtained simultaneously and which is free of the aforementioned orthogonality issue. While the REKS and SA-REKS Φ_{CT} energy profiles are virtually the same, the SA-REKS Φ_{DIR} state is shifted by 2 to 5 kcal/mol with respect to Φ_{CT}. This modified energy difference shifts the crossing point to the BLA value ~0.033.

Using the BH&HLYP instead of HF, that is, reducing the amount of Hartree−Fock exchange to 50% and adding the LYP correlation functional, modifies only the relative energies of the Φ_{CT} profiles, the latter remaining parallel along the BLA path. The situation is somewhat different for the Φ_{DIR} energy profiles. When carrying out separate REKS calculations for the Φ_{CT} and Φ_{DIR} states, the calculation for the Φ_{DIR} state could not be converged for the values of the BLA coordinate below −0.005, because, in this region, the Φ_{DIR} state becomes an excited state and the energy gap between Φ_{CT} and Φ_{DIR} is larger than 10 kcal/mol. SA-REKS helps to overcome this issue; however, both states

dx.doi.org/10.1021/ct4003465 | J. Chem. Theory Comput. 2013, 9, 3917−3932

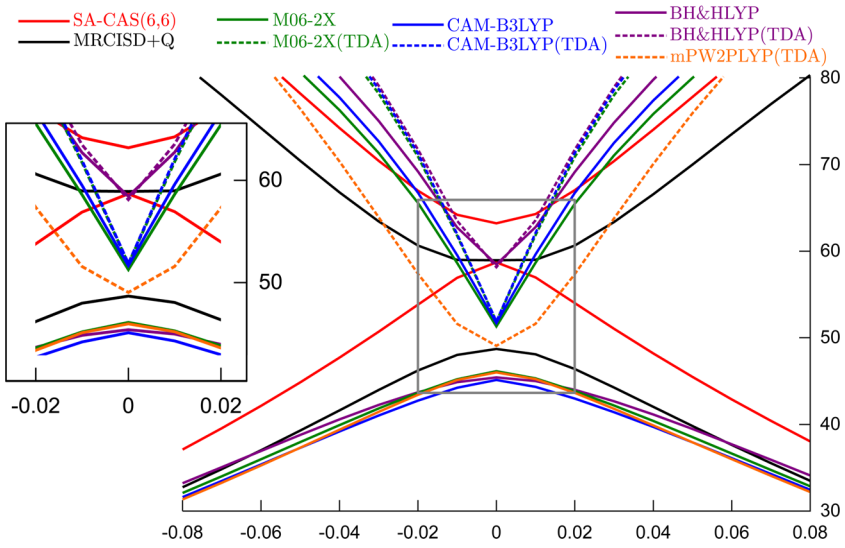

Figure 4. SA-CAS(6,6), MRCISD+Q and DFT/TDDFT S_0 and S_1 energy profiles (in kcal/mol) along MEP_{CT}.

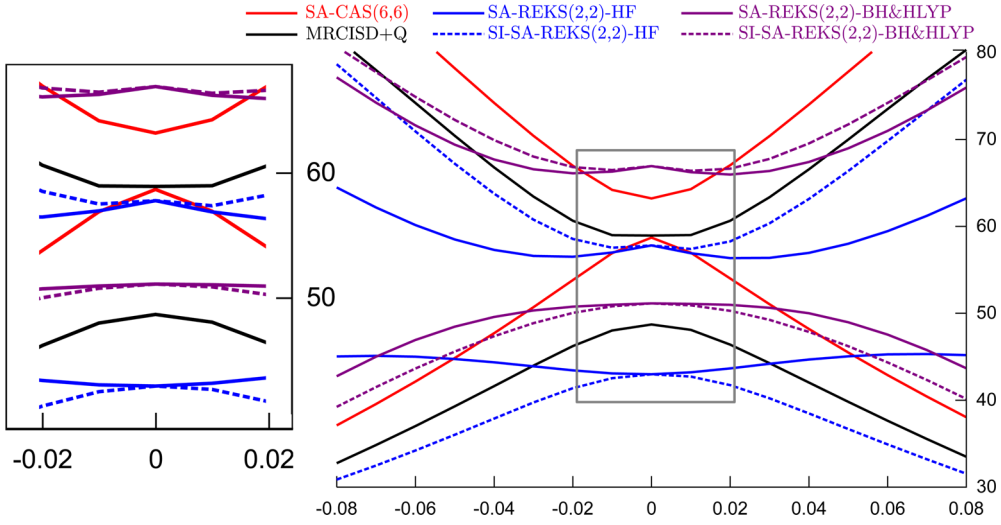

Figure 5. SA-CAS(6,6), MRCISD+Q, and SA-REKS S_0 and S_1 energy profiles (in kcal/mol) along MEP_{CT}.

are destabilized by ca. 7 kcal/mol due to the orbital optimization for an averaged state. Because this energy shifting is rather similar for both states, their extrapolated intersections both occur between the BLA values of 0.04 and 0.05. Finally, note a good agreement between the REKS and MRCISD+Q Φ_{DIR} energy profiles, similar to what has been observed using BH&HLYP-(TDA), indicating that this functional would be suitable in the modeling of PSB3 photochemistry.

4.2. MEP_{CT}. MEP_{CT} has been constructed to investigate the profile of the ground state PES of PSB3 in the forward and backward directions of the pathway connecting the TS_{CT} geometry with the *trans* and *cis* conformations, respectively. Figure 4 shows the same region of PES obtained using DFT and TDDFT methods, as well as the reference SA-CAS(6,6) and MRCISD+Q data. The full response TDDFT as well as the TDA approaches are considered when available.

Note that, for all the density functionals employed, the TDDFT excitation energies are positive, indicating that the closed shell Φ_{CT} configuration remains the ground state along the full length of the path. Furthermore, the energy profiles of the S_0 state obtained in the DFT calculations are almost parallel to the MRCISD+Q reference profile, and at the TS_{CT} geometry, they lie ca. 45 kcal/mol above the energy of the *cis* conformation. The situation is different for the excited state, that is, the state exhibiting the largest multireference character. All the functionals, except the double-hybrid mPW2PLYP(TDA), feature a pronounced cusp at the TS_{CT} geometry, in a visible contradiction with the smooth SA-CAS(6,6) and MRCISD+Q curves. The presence of the cusp suggests a wrong description of the interaction between the Φ_{DIR} and Φ_{CT} configurations. While M06-2X and CAM-B3LYP give similar S_1 profiles, resulting in an energy gap of only 5 kcal/mol at TS_{CT} close to the SA-CAS(6,6) one, the BH&HLYP ΔE is significantly larger (13 kcal/mol), in a better agreement with MRCISD+Q. Using TDDFT(TDA), the Φ_{DIR} profiles near the TS_{CT} geometry are only slightly affected. However, the TDA effect becomes more pronounced when the PSB3 geometry differs significantly from TS_{CT}, in relation with the increasing delocalization of the φ_N and φ_C orbitals. Finally, the use of the double-hybrid functional has a dramatic effect on the S_1 profile. The energy gap at TS_{CT} is the smallest one, only 3 kcal/mol. However, it seems that its slope near TS_{CT} is less peaked than the ones observed with the other functionals, indicating that the perturbative addition of double excitations via the CIS(D) scheme[57,58] may be able to recover some amount of

dx.doi.org/10.1021/ct4003465 | J. Chem. Theory Comput. 2013, 9, 3917−3932

interaction between the Φ_{CT} and Φ_{DIR} configurations. Nevertheless, note that the energy gap still increases too rapidly along the MEP coordinate.

The SA-REKS results using the HF and BH&HLYP XC functionals are shown in Figure 5. As obtained from the analysis of the φ_N and φ_C orbital occupations, the ground electronic state is dominated by the Φ_{CT} configuration and the excited state is dominated by the Φ_{DIR} configuration. It is noteworthy that, without applying the SI-SA-REKS procedure (see section 3), the SA-REKS S_0 and S_1 PES profiles do not consistently follow the reference MRCISD+Q profiles. With the use of both XC functionals, there is a very shallow energy barrier near the TS_{CT} geometry on the excited state PES. This can be attributed to the combined effect of two factors: the use of the geometries optimized in the CASSCF calculations and a much too restrictive character of the excited state electronic configuration (pure diradicaloid state) in the SA-REKS energy functional (eq 10). Allowing the ground and the excited SA-REKS states to interact via the SI-SA-REKS procedure considerably improves the shape of the PES profiles (shown with dashed lines in Figure 5) and brings them in a close agreement with the reference ones. A tiny barrier on the order of 0.1 kcal/mol still persists on the SI-SA-REKS excited state PES profiles.

Comparison of the REKS S_0 and S_1 PES profiles in Figure 5 with the TDDFT profiles in Figure 4 shows the importance of the configuration interaction (lacking in TDDFT excited states) to properly describe the multireference character of the S_1 state. The cusp on the S_1 PES near the TS_{CT} geometry produced by the TDDFT calculations disappears and the SI-SA-REKS profiles are in a qualitative agreement with the MRCISD+Q ones. The energy gap at the TS_{CT} geometry obtained in the SI-SA-REKS/BH&HLYP calculation amounts for 15.8 kcal/mol, in a good agreement with the MRCISD+Q gap of 10.2 kcal/mol. On the other hand, the TDDFT gaps range from 3.1 to 13.3 kcal/mol. Accordingly, the SI-SA-REKS and TDDFT results bracket the reference value.

Mulliken atomic charges of the allyl moiety (see Figure 6) obtained from the SA-CAS(6,6) and MRCISD reveal that the Φ_{CT} electronic configuration is dominant in the ground state only in the close vicinity of the TS_{CT} geometry.[1] Sharp peaks of the SA-CAS(6,6) and MRCISD curves shown in Figure 6 reflect a strong localization of the positive charge on the allyl moiety near the TS_{CT} geometry. Beyond the IRC values of ±0.05 Å·amu$^{1/2}$, the Φ_{DIR} electronic configuration becomes dominant in the S_0 state and the overall charge on the allyl moiety returns to the values typical for the planar *cis* conformation. Analysis of the Mulliken charges obtained in the DFT calculations shows a considerably reduced localization of the positive charge on the allyl moiety near the TS_{CT} geometry. This can be attributed to a well-known tendency of the approximate density functionals to yield overly delocalized density distribution due to the inherent electron self-interaction error.[60,61] Thus, the magnitude of the overall charge transfer from the Schiff base to the allyl moiety in the ground state of PSB3 as obtained in the DFT calculations does not provide a clear distinction between the regions on the MEP_{CT} pathway where the Φ_{CT} or Φ_{DIR} electronic configuration dominates the S_0 state.

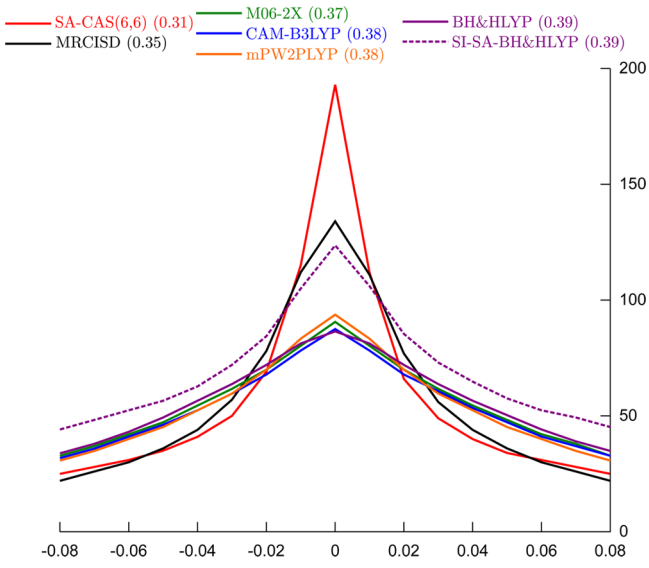

Figure 6. SA-CAS(6,6), MRCISD, DFT, and SA-REKS (using averaged orbitals) S_0 Mulliken charge transfer (with respect to the *cis* conformation reported in parentheses, in %) along MEP_{CT}.

The use of the Mulliken charges to analyze the electronic structure of the S_0 and S_1 states produced by the SI-SA-REKS calculations is hampered by the absence of the relaxed density matrix for the individual states (see section 3). Although the overall Mulliken charge of the allyl moiety of PSB3 in the S_0 state calculated using the SI-SA-REKS orbitals only (see Figure 6) follows the same trend as the other DFT methods, a fair comparison with the MRCISD results cannot be done at the moment and needs to be postponed until the relaxed density matrix calculations for the individual states will be implemented in the SI-SA-REKS method. On the other hand, the orbital occupation numbers (Figure S2, see the Supporting Information) confirm the closed-shell character of the ground state while the first excited state is characterized by occupation numbers varying between 1.5 and 1.0 for one active orbital and the complement to 2.0 for the other one, as expected for a state with a large multiconfigurational character.

4.3. MEP_{DIR}. Following Gozem et al.,[1] the geometries for the MEP_{DIR} pathway were generated from the ground state thermal isomerization pathway connecting the *cis* conformation to the *trans* conformation of PSB3 via TS_{DIR}. The SA-CAS(6,6) calculations predict that, along the whole MEP_{DIR} pathway, the ground state electronic structure of PSB3 is mainly diradicaloid. The S_1 state has a Φ_{CT} character, and at the TS_{DIR} geometry, it lies 7.4 kcal/mol above the S_0 state. Inclusion of the dynamic electron correlation in the MRCISD+Q method narrows the S_1-S_0 gap down to only 0.6 kcal/mol.

The DFT S_0 and TDDFT S_1 energy profiles along the MEP_{DIR} pathway are shown in Figure 7. Qualitatively, the S_0 and S_1 profiles look very similar to the ones obtained in the DFT and TDDFT calculations for the MEP_{CT} pathway. Irrespective of the density functional employed, both the ground and the excited state energy profiles feature cusps near the TS_{DIR} geometry, which, most likely, is a consequence of the absence of interaction between the Φ_{DIR} and Φ_{CT} configurations. All functionals except BH&HLYP show an imaginary excitation at TS_{DIR}, consistent with the fact that the corresponding Φ_{CT} and Φ_{DIR} profiles cross before the TS_{DIR} geometry along the BLA pathway.

The Mulliken analysis along this path is based on the corresponding S_0 density, even when the Φ_{DIR} configuration dominates. In all the packages used in this study, there is no possibility to carry out the Mulliken analysis of the TDDFT-(TDA) density matrix; however, it may be expected that the TDDFT(TDA) Mulliken charges follow similar trends to the TDDFT ones. Hence, in Figure 8, only the full TDDFT Mulliken

dx.doi.org/10.1021/ct4003465 | J. Chem. Theory Comput. 2013, 9, 3917−3932

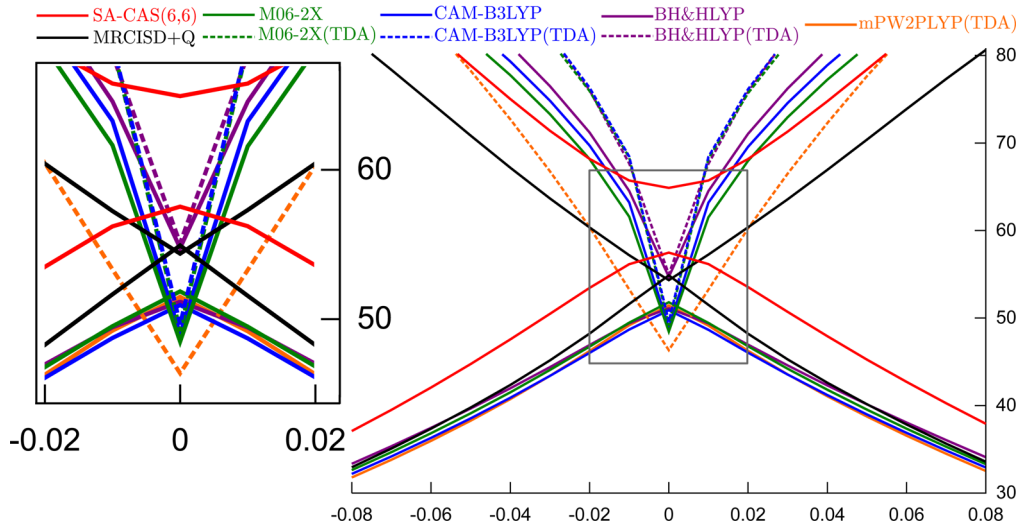

Figure 7. SA-CAS(6,6), MRCISD, and DFT/TDDFT S_0 and S_1 energy profiles (in kcal/mol) along MEP_{DIR}.

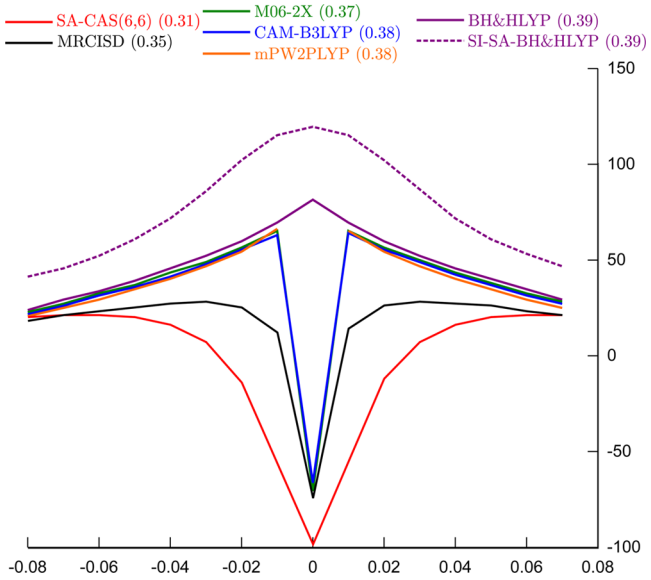

Figure 8. SA-CAS(6,6), MRCISD, DFT (or TDDFT), and SA-REKS (using averaged orbitals) Mulliken charge transfer (with respect to the *cis* conformation reported in parentheses, in %) along MEP_{DIR}. Note that the reported charge change at coordinate 0 has been obtained at the TDDFT level of theory for BH&HLYP, M06-2X, and CAM-B3LYP functionals.

charges for CAM-B3LYP and M06-2X functionals are reported for the TS_{DIR} structure. The Mulliken analysis (Figure 8) shows that the DFT electronic structures for geometries different from TS_{DIR} are characterized by a strong and slowly varying charge transfer, at variance with the more pronounced changes obtained with SA-CAS(6,6) and MRCISD. Again, by construction KS-DFT gives access to pure Φ_{CT} state, explaining why the charge transfer character remains high all along the path. However, at the point of imaginary excitation (TS_{DIR}), the TDDFT state becomes the lowest, as shown by the sudden change of the S_0 allyl Mulliken charge.

The SA-REKS MEP_{DIR} energy profiles obtained using the BH&HLYP and HF XC functionals are reported in Figure 9. Within the range of geometries optimized using the SA-CAS(6,6) method for the BLA, MEP_{CT}, and MEP_{DIR} pathways, the ground electronic state predicted by the SA-REKS method is dominated by the Φ_{CT} electronic structure. The extrapolated crossing point on the SA-REKS/BH&HLYP BLA curve (see Figure 3) is shifted beyond the range of geometries optimized with SA-CAS(6,6), such that, at the TS_{DIR} geometry, the ground electronic state as predicted by the SA-REKS calculations retains the Φ_{CT} character. In this respect, the SA-REKS results are similar to the QD-NEVPT2 results obtained by Gozem et al.[1] At variance with the TDDFT calculations, the shapes of the S_0 and S_1 PES profiles obtained in the SI-SA-REKS/BH&HLYP and SI-SA-REKS/HF calculations are smooth and follow sufficiently closely the reference MRCISD+Q curves.

4.4. Analysis of Differences between DFT and Wave Function Methods. In the previous sections, we presented data along three scans for several representative DFT methods. These data deserve a further analysis, thanks to a fair comparison between wave function-based (CASSCF, MRCISD) approaches and DFT-based ones (KS-DFT, TDDFT, REKS). In the latter, it is assumed that a major part of the electronic correlation can be qualified as dynamic, with only the REKS(2,2) approach including some static correlation thanks to its fractional occupations of the HOMO and LUMO orbitals.

At variance with DFT results, the multiconfigurational wave function-based reference data have been obtained using the full set of π orbitals in the active space. Such an active space in the CASSCF calculations enables one to take into account not only the static correlation effects, as represented by the natural orbitals (φ_N and φ_C in Ψ_{DIR}) with the occupation numbers significantly different from 0 or 2, but also an unspecified fraction of the dynamic correlation effects, as represented by the nearly doubly occupied or nearly empty natural orbitals. Then, a more complete account of the dynamic electron correlation is achieved with the use of the MRCISD+Q method. Hence, limiting the size of the active space to φ_N and φ_C orbitals (Figure 1) allows to capture static correlation effects within a configurational space more similar to the ones found in REKS(2,2) and TDDFT approaches. In the following, the corresponding CASSCF and MRCISD+Q calculations will be denoted as SA-CAS(2,2) and MRCISD+Q(2,2).

We report the energy profiles along the BLA, MEP_{CT}, and MEP_{DIR} pathways recomputed using the SA-CAS(2,2) and MRCISD+Q(2,2) methods and compare them with the SA-CAS(6,6) and MRCISD+Q ones and also the TDDFT and

dx.doi.org/10.1021/ct4003465 | J. Chem. Theory Comput. 2013, 9, 3917−3932

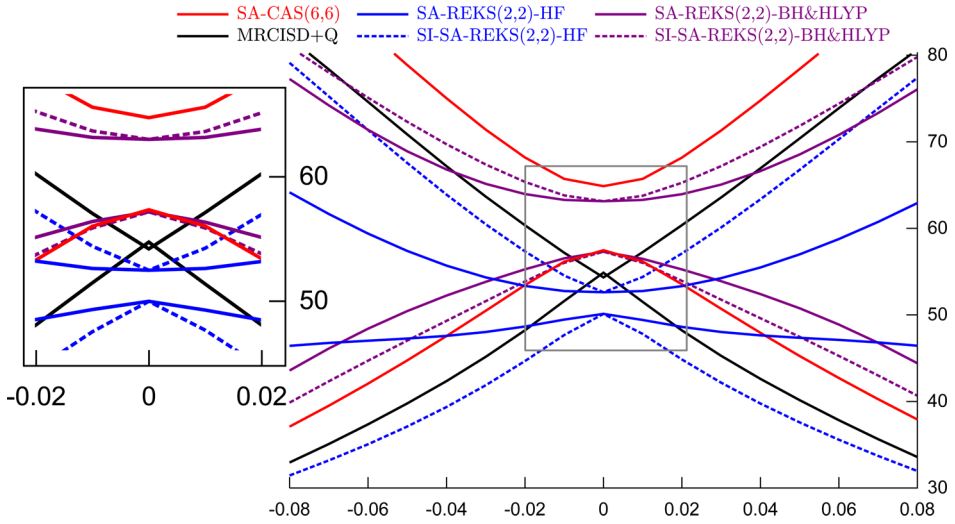

Figure 9. SA-CAS(6,6), MRCISD, and SA-REKS S_0 and S_1 energy profiles (in kcal/mol) along MEP_{DIR}.

REKS energy profiles, using BH&HLYP only. In these calculations, the molecular geometries obtained at the SA-CAS(6,6) level are employed. All the energy profiles and changes in the PSB3 allyl moiety Mulliken charge are shown in Figure 10.

In the case of the BLA pathway (Figure 10a), the use of a reduced (2,2) active space leads to a 2−3 kcal/mol destabilization of the diradical state while the charge transfer state is stabilized by almost 10 kcal/mol relative to the SA-CAS(6,6) curves. This causes a considerable displacement of the extrapolated crossing position toward a more positive value of the BLA coordinate as compared to the SA-CAS(6,6) method. However, the MRCISD+Q results are less affected by the size of the active space, and the position of the crossing is only slightly shifted to a more positive value of the BLA coordinate. It is noteworthy that the crossing point at the SA-CAS(2,2) level occurs near the same BLA value as the MRCISD+Q or the MRCISD+Q(2,2) crossing points.

Comparison with DFT and SI-SA-REKS intersection topologies evidence a qualitative agreement: except in the SA-CAS(6,6) case, all the crossing topologies are sloped and occur at BLA coordinate value confined between 0.025 and 0.050. Moreover, the BH&HLYP intersection point energy is very close to the MRCISD+Q one (whatever the chosen active space), whereas the SI-SA-REKS overestimates it by about 10 kcal/mol.

The MRCISD+Q energy profiles along MEP_{CT} shown in Figure 10b are largely insensitive to the size of the active space. The ground state in the vicinity of TS_{CT} has the charge transfer character, as shows the analysis of the allyl Mulliken charges. Its magnitude is reduced when a minimal active space is used, especially at the CASSCF level of theory, echoing the significant increase of the energy gap when going from SA-CAS(6,6) to SA-CAS(2,2).

The shape of the DFT-based CT energy profiles, as well as the corresponding Mulliken charge distribution, are closer to the SA-CAS(2,2) and MRCISD+Q(2,2) ones than to the larger active space counterparts. These results confirm a very similar electronic structure between DFT and (2,2)-based multireference methods. Regarding the DIR state, the DFT results are less conclusive. As already mentioned, the TDDFT excited state does not interact with the ground state, resulting in a peaked S_1 energy profile, while the SI-SA-REKS exhibits a qualitatively correct shape. Moreover, it is noteworthy that SI-SA-REKS compares better with SA-CAS(2,2) and MRCISD+Q(2,2), highlighting again the importance of the active space.

For MEP_{DIR} (Figure 10c), the quality of the ground state has a stronger dependence on the size of the active space. While S_0 at the TS_{DIR} geometry has the diradical character at the SA-CAS(6,6) and the MRCISD+Q levels of theory, it is striking that the SA-CAS(2,2) and the MRCISD+Q(2,2) methods yield the charge transfer ground state. This reflects the fact that TS_{DIR} is geometrically close to an intersection point and a change of theory may result in a change of the ground state electronic structure. Because the geometry optimization at the MRCISD+Q level can be too time-consuming, the reported energy profiles suggest that the geometry optimized at the SA-CAS(2,2) level of theory may be used instead.

Similarly to MEP_{CT}, the CT energy profile along MEP_{DIR} is correctly described using DFT approaches, again with a closer agreement to SA-CAS(2,2) and MRCISD+Q(2,2) results as reflected by the charge distribution. However, the overestimation and the slow variation of the DFT Mulliken charge firmly demonstrate the lack of interaction of Φ_{CT} with Φ_{DIR} at this level of theory.

4.5. Role of the Electronegativities of the Allyl and Protonated Schiff Base Moieties. From the presented results, it is clear that the shape of the ground and excited state PESs along the MEP_{CT}, MEP_{DIR}, and BLA pathways depends strongly on the relative stability of the electronic states dominated by the Φ_{CT} and Φ_{DIR} electronic configurations. The latter, in turn, can be rationalized using the relative electronegativity of the fragments connected by the C_2-C_3 bond,[54,62] that is the Schiff base and the allyl fragments of PSB3. Indeed, when two fragments with approximately equal electronegativities are connected by a double bond (such as C=C bond in ethylene), twisting about this bond results in a homolytic breaking of its π-component via a diradical transition state for such a bond breaking.[54,62] When the two fragments have very different electronegativities, such as in PSB3 cation, the heterolytic breaking of the double bond becomes nearly isoenergetic with the homolytic one and may even become the preferred mechanism provided that the electronegativity difference is sufficiently large.[54,62] The SA-CAS(6,6) energy profiles (see for instance the solid red lines in Figure 10a) indicate that the two π-bond breaking mechanisms are nearly isoenergetic and the CI occurs slightly above the energy levels of the two transition states,

dx.doi.org/10.1021/ct4003465 | J. Chem. Theory Comput. 2013, 9, 3917−3932

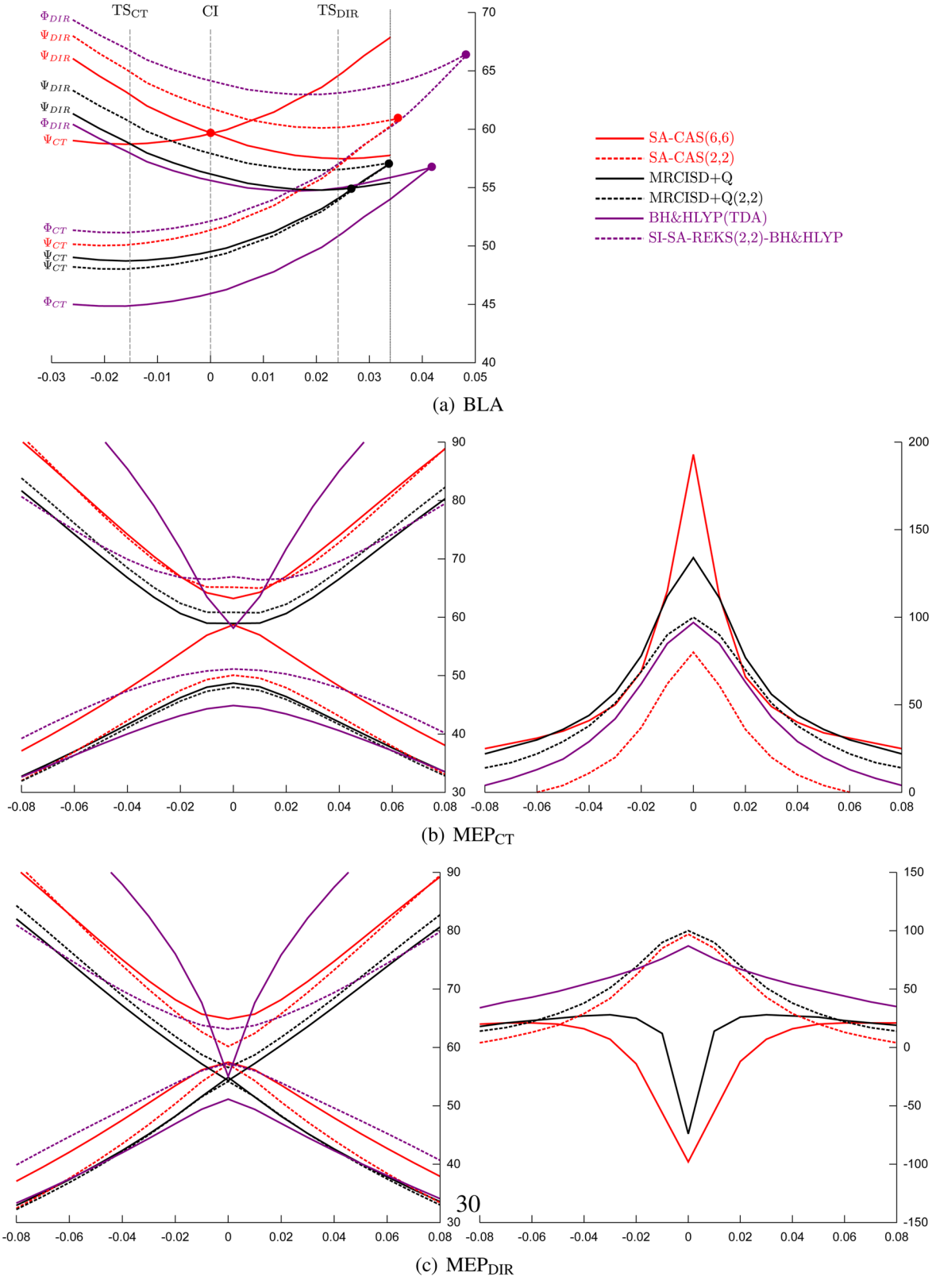

Figure 10. SA-CAS(6,6), SA-CAS(2,2), MRCISD+Q, and MRCISD+Q(2,2) S_0 and S_1 energy profiles (left panel, in kcal/mol) and Mulliken charge transfer (without the Davidson correction, with respect to the *cis* conformation, right panel, in %) along the three MEPs. Crossing points are indicated with filled circles. The positions of TS_{CT}, TS_{DIR}, and the conical intersection (obtained at the SA-CAS(6,6) level of theory) are also reported in the case of the BLA pathway.

TS_{DIR} and TS_{CT} . The inclusion of the dynamic electron correlation via the MRCISD method leads to a stabilization of the TS_{CT} structure relative to TS_{DIR}, which implies that, at this level of theory, the Schiff base fragment becomes more electronegative relative to the allyl fragment than at the CASSCF level. The stabilization of the TS_{CT} structure is further increased

dx.doi.org/10.1021/ct4003465 | J. Chem. Theory Comput. 2013, 9, 3917−3932

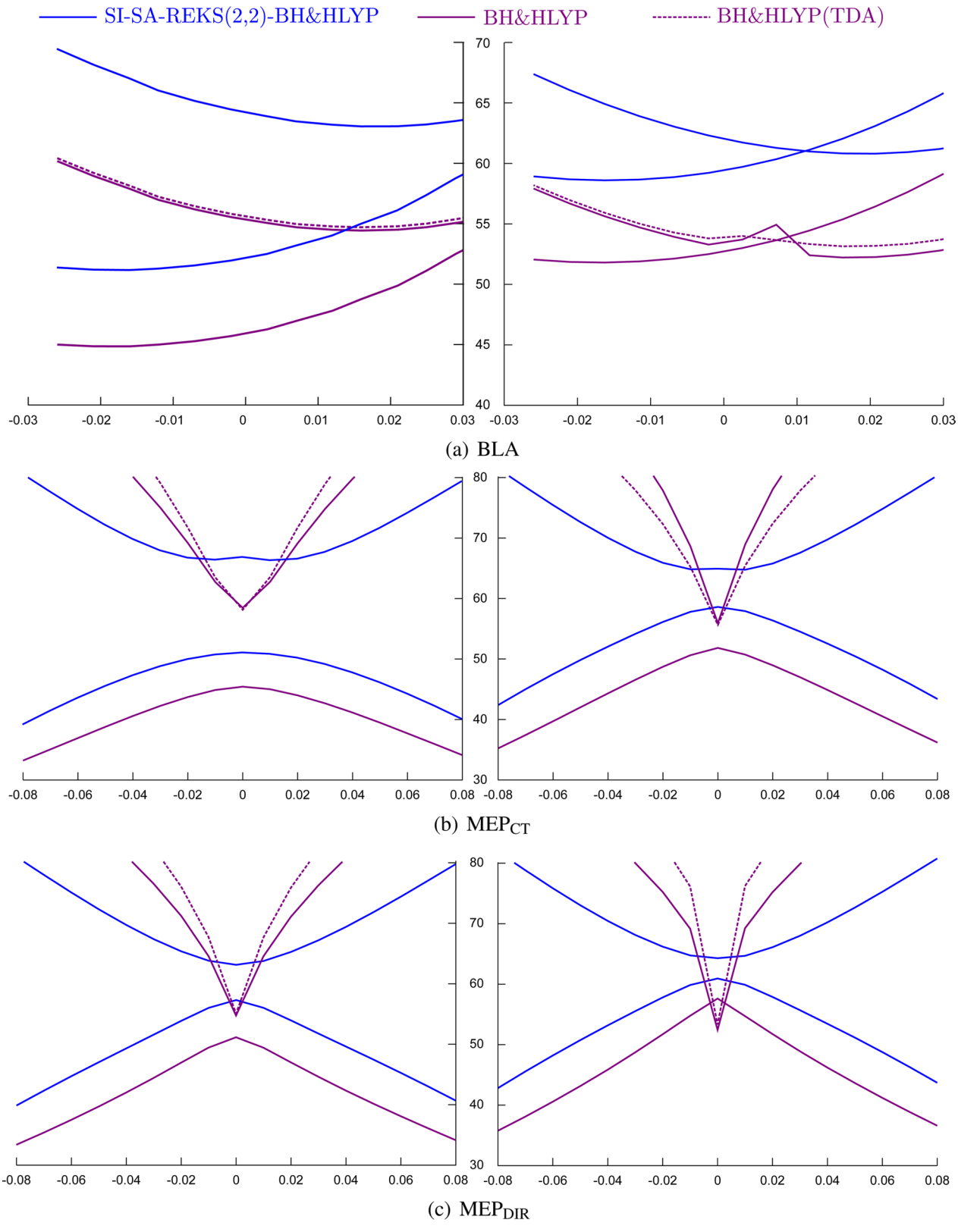

Figure 11. S_0 and S_1 energy profiles along the BLA, MEP$_{CT}$, and MEP$_{DIR}$ paths, obtained at different DFT levels of theory, using either no electric field (left) or a −0.004 au electric field applied along the molecular axis (right).

by the inclusion of the size extensivity correction in the MRCISD +Q method and the crossing, at this level of theory, occurs virtually at the TS$_{DIR}$ structure. To demonstrate that it is the balance of electronegativities of the allyl and the Schiff base fragments that determines the shape of the ground and excited state PESs along the BLA, MEP$_{CT}$, and MEP$_{DIR}$ pathways, we have undertaken an additional set of calculations using the SI-SA-REKS(2,2) and the TDDFT methods using the BH&HLYP

dx.doi.org/10.1021/ct4003465 | J. Chem. Theory Comput. 2013, 9, 3917−3932

functional. In the new calculations, a weak electric field of −0.004 au is applied along the molecular axis. The action of the field slightly destabilizes the ionic Φ_{CT} configuration with respect to the covalent Φ_{DIR} configuration. The results of the new calculations are summarized in Figure 11 along with the results of the field-free calculations using the same methods.

As it can be seen in the case of the BLA coordinate in Figure 11, the shapes of the TDDFT and SI-SA-REKS PES profiles are only slightly affected by the external field. However, the relative positions of the Φ_{CT} and Φ_{DIR} energy profiles are modified, while the Φ_{CT} profile is destabilized by 6 to 7 kcal/mol with respect to the field-free profile, the Φ_{DIR} one is stabilized by 2 to 3 kcal/mol. Consequently, the Φ_{CT} and Φ_{DIR} profiles now cross at the values of the BLA coordinate of 0.009 Å and 0.012 Å for TDDFT and SI-SA-REKS, respectively. After the crossing point, the SI-SA-REKS ground state becomes diradicaloid. Along the MEP_{DIR} pathway, the ground electronic state, according to the SI-SA-REKS calculations, remains diradicaloid between the IRC values of $\pm$0.02 Å·amu$^{1/2}$ around the TS_{DIR} geometry, as demonstrated by the orbital occupation numbers (see Figure S3, Supporting Information). This agrees closely with the MRCISD+Q results for this pathway. It is noteworthy that, at the TDDFT and TDDFT(TDA) levels of theory, the Φ_{DIR} state "crashes" into the Φ_{CT} state as one follows the MEP_{DIR} pathway. A similar behavior of the TDDFT excited states was already reported for the H_3 molecular system.[7] Finally, the MEP_{CT} profile remains largely unaffected by the application of the field.

From the results presented in Figure 11, it can be conjectured that the major source of difference between the multireference wave function calculations and the REKS calculations lies in the description of the relative stabilities of the Φ_{CT} and Φ_{DIR} electronic configurations. Because the use of the BH&HLYP density functional yields a noticeable preference for the Φ_{CT} electronic configuration in the ground state of PSB3, the crossing between the S_0 and S_1 states occurs farther along the BLA pathway than is predicted by the SA-CAS(6,6) and MRCISD+Q calculations.

5. CONCLUSIONS

In this study, following the seminal work by Martinez and co-workers,[7] we have used DFT-based calculations (KS-DFT, TDDFT, and REKS) to describe three potentially important regions in the isomerization of the retinal model system, PSB3. While the Φ_{CT} configuration is easily described with standard KS-DFT approaches, linear-response TDDFT calculations are required to reach the multideterminantal Φ_{DIR} configuration. It is noteworthy that, in certain circumstances (corresponding to an imaginary or negative excitation), the former can be an excited state while the latter is actually the ground state. Alternatively, the REKS approach can be used to reach any of these two configurations, which can be described by different sets of HOMO and LUMO occupations.

In its current state of development, the usual linear-response TDDFT cannot be recommended for black-box investigations of the potential energy surfaces of molecular systems undergoing bond rearrangements, such as the isomerization of PSB3. Because the Φ_{DIR} and Φ_{CT} states do not interact in the TDDFT approach, the position of the state crossing will depend on their relative stabilities which, in turn, is highly dependent on the chosen DFT functional. At the point of degeneracy, the DFT calculations are not easily converged due to the breakdown of the pure-state v-representability. Only the double-hybrid functional slightly mitigates this problem. In the situations when the ground state can be faithfully described by a single Kohn−Sham determinant, such as the rearrangement of PSB3 along the MEP_{CT} pathway, a wrong profile of the excited state PES is obtained, due to the lack of interaction between Φ_{DIR} and Φ_{CT}. Nevertheless, the ground state is qualitatively well described, as can be judged from the shape of the energy profile and the character of the state. The wrong description of the Φ_{DIR} state is exacerbated by the presence of the strong nondynamic electron correlation in the ground state, such as in the case of the MEP_{DIR} pathway. Near the crossing between the ground and the excited states, the TDDFT description leads to certain artifacts manifested by kinks on the excited state PES (e.g., see Figure 11). The amplitude of kinks can be reduced by the use of the Tamm−Dancoff approximation; however, the TDDFT(TDA) method shows the same artifacts as the full response TDDFT. Partly, the deficiencies of the TDDFT calculations carried out using the conventional GGA and hybrid density functionals can be corrected by the use of the double hybrid density functionals. More seriously, the absence of state interaction even leads to a qualitatively wrong description when S_0 corresponds mainly to Φ_{DIR}, such at TS_{DIR}. Consequently, no Φ_{DIR} transition state can exist at this level of theory.

The use of the SA-REKS (and SI-SA-REKS) method leads to a reasonable agreement with the reference MRCISD+Q data. The shapes of the ground and the excited state PESs along the BLA, MEP_{DIR}, and MEP_{CT} pathways are sufficiently accurately reproduced by the SA-REKS calculations. It should, however, be noted that the occurrence of state crossing and the transitions states for the homolytic and the heterolytic mechanism of the breaking of the C_2-C_3 bond of PSB3 (see Figure 1) depends critically on the relative stability of the covalent (Φ_{DIR}) and the ionic (Φ_{CT}) electronic configurations.[62] Indeed, their relative stability has been found to be dependent on the method according to the multireference methods used to generate the benchmark data in ref 1 and by the density functionals employed in the present work in connection with REKS. While the SA-CAS(6,6) calculations yield a slight preference in favor of the Φ_{DIR} electronic configuration, the MRCISD+Q method makes the Φ_{CT} configuration more stable.

Altering the relative stability of the Φ_{DIR} and Φ_{CT} configurations by the application of a weak electric field brings the DFT results in a closer agreement with the benchmark MRCISD+Q data. This observation underlines the importance of a balanced and correct description of the dynamic correlation effects, which are responsible for the relative stability of the covalent and the ionic configurations. At the multireference *ab initio* level of theory the relative stability of these configurations depends on many factors such as the size of the active space, the size of the basis set, and the molecular geometry employed. Preferably, the reference benchmark data are to be obtained using sufficiently large basis set or extrapolated to the basis set limit by the use of a systematically convergent sequence of the basis sets with the MRCISD+Q method. The observed close agreement between the SA-CAS(2,2) and the MRCISD+Q methods (due to error compensations) suggests that a reduced active space could be employed in the multireference *ab initio* calculations for obtaining the molecular geometries. Further investigations are required in order to assess the general validity of this last observation (with respect to other basis sets and to larger parts of the potential energy surfaces).

■ ASSOCIATED CONTENT

Supporting Information

The BLA energy profile using the mPW2PLYP functional, with or without the perturbative correction to the ground state energy. SI-SA-REKS active orbital occupation numbers along the three paths. All the computed energies and the allyl Mulliken charges along the three paths. This material is available free of charge via the Internet at http://pubs.acs.org/.

■ AUTHOR INFORMATION

Corresponding Author

*E-mail: miquel.huix-rotllant@univ-amu.fr; mike.filatov@gmail.com; molivuc@bgsu.edu; nicolas.ferre@univ-amu.fr.

Notes

The authors declare no competing financial interest.

■ ACKNOWLEDGMENTS

M.H.-R. and N.F. thank ANR project "Impact", ANR-11-BS08-0016, for funding, the Centre Régional de Ressources en Modélisation Moléculaire and the Mésocentre d'Aix-Marseille Université for computational resources. M.F. acknowledges financial support provided by the European Union Seventh Framework Programme (FP7/2007-2013) under the IEF Grant Agreement No. 326652. M.O. is grateful to the National Science Foundation for Grant Nos. CHE-1152070, to the Human Frontier Science Program Organization for Grant No. RGP0049/2012CHE09-56776, and to NSF TeraGrid for granted computer time. The COST-CMTS Action CM1002 "Convergent Distributed Environment for Computational Spectroscopy (CODECS)" is also acknowledged.

■ REFERENCES

(1) Gozem, S.; Huntress, M.; Schapiro, I.; Lindh, R.; Granovsky, A. A.; Angeli, C.; Olivucci, M. *J. Chem. Theory Comput.* **2012**, *8*, 4069−4080.
(2) Gozem, S.; Krylov, A. I.; Olivucci, M. *J. Chem. Theory Comput.* **2013**, *9*, 284−292.
(3) Kohn, W.; Sham, L. J. *Phys. Rev.* **1965**, *140*, A1133−A1138.
(4) Cohen, A. J.; Handy, N. C. *Mol. Phys.* **2001**, *99*, 607−615.
(5) Cremer, D. *Mol. Phys.* **2001**, *99*, 1899−1940.
(6) Baer, R. *Phys. Rev. Lett.* **2010**, *104*, 073001.
(7) Levine, B. G.; Ko, C.; Quenneville, J.; Martínez, T. J. *Mol. Phys.* **2006**, *104*, 1039−1051.
(8) Cordova, F.; Doriol, L. J.; Ipatov, A.; Casida, M. E.; Filippi, C.; Vela, A. *J. Chem. Phys.* **2007**, *127*, 164111.
(9) Peach, M. J. G.; Williamson, M. J.; Tozer, D. J. *J. Chem. Theory Comput.* **2011**, *7*, 3578−3585.
(10) Tajkhorshid, E.; Suhai, S. *Chem. Phys. Lett.* **1999**, *299*, 457−464.
(11) Tajkhorshid, E.; Suhai, S. *J. Mol. Struct.: THEOCHEM* **2000**, *501*−*502*, 297−313.
(12) Röhrig, U. F.; Guidoni, L.; Laio, A.; Frank, I.; Röthlisberger, U. *J. Am. Chem. Soc.* **2004**, *126*, 15328−15329.
(13) Sugihara, M.; Buss, V.; Entel, P.; Elstner, M.; Frauenheim, T. *Biochemistry* **2002**, *41*, 15259−15266.
(14) Zhou, H.; Tajkhorshid, E.; Frauenheim, T.; Suhai, S.; Elstner, M. *Chem. Phys.* **2002**, *277*, 91−103.
(15) Okada, T.; Sugihara, M.; Bondard, A.-N.; Elstner, M.; Entel, P.; Buss, V. *J. Mol. Biol.* **2004**, *342*, 571−583.
(16) Torii, H. *J. Am. Chem. Soc.* **2002**, *124*, 9272−9277.
(17) Nakajima, S.; Ohno, K.; Inoue, Y.; Sakurai, M. *J. Phys. Chem. B* **2003**, *107*, 2867−2874.
(18) Gascon, J. A.; Batista, V. S. *Biophys. J.* **2004**, *87*, 2931−2941.
(19) Touw, S. I. E.; de Groot, H. J. M.; Buda, F. *J. Phys. Chem. B* **2004**, *108*, 13560−13572.
(20) Wanko, M.; Garavelli, M.; Bernardi, F.; Niehaus, T. A.; Frauenheim, T.; Elstner, M. *J. Chem. Phys.* **2004**, *120*, 1674−1692.
(21) Fantacci, S.; Migani, A.; Olivucci, M. *J. Phys. Chem. A* **2004**, *108*, 1208−1213.
(22) Aquino, A. J. A.; Barbatti, M.; Lischka, H. *ChemPhysChem* **2006**, *7*, 2089−2096.
(23) Send, R.; Sundholm, D. *J. Phys. Chem. A* **2007**, *111*, 27−33.
(24) Send, R.; Sundholm, D. *J. Phys. Chem. A* **2007**, *111*, 8766−8773.
(25) Altun, A.; Yokoyama, S.; Morokuma, K. *J. Phys. Chem. B* **2008**, *112*, 6814−6827.
(26) Chiba, M.; Tsuneda, T.; Hirao, K. *J. Chem. Phys.* **2006**, *124*, 144106.
(27) Send, R.; Sundholm, D.; Johansson, M. P.; Pawlowski, F. *J. Chem. Theory Comput.* **2009**, *5*, 2401−2414.
(28) Rostov, I. V.; Amos, R. D.; Kobayashi, R.; Scalmani, G.; Frisch, M. J. *J. Phys. Chem. B* **2010**, *114*, 5547−5555.
(29) Valsson, O.; Angeli, C.; Filippi, C. *Phys. Chem. Chem. Phys.* **2012**, *14*, 11015−11020.
(30) Valsson, O.; Filippi, C. *J. Phys. Chem. Lett.* **2012**, *3*, 908−912.
(31) Seidl, A.; Görling, A.; Vogl, P.; Majewski, J. A.; Levy, M. *Phys. Rev. B* **1996**, *53*, 3764−3774.
(32) Perdew, J. P.; Schmidt, K. *AIP Conf. Proc.* **2001**, *577*, 1−20.
(33) Bernard, Y. A.; Shao, Y.; Krylov, A. I. *J. Chem. Phys.* **2012**, *136*, 204103.
(34) Xu, X.; Gozem, S.; Olivucci, M.; Truhlar, D. G. *J. Phys. Chem. Lett.* **2013**, *4*, 253−258.
(35) Lieb, E. H. *Int. J. Quantum Chem.* **1983**, *24*, 243−277.
(36) (a) Englisch, H.; Englisch, R. *Phys. Status Solidi B* **1984**, *123*, 711−721. (b) Englisch, H.; Englisch, R. *Phys. Status Solidi B* **1984**, *124*, 373−379.
(37) Ullrich, C. A.; Kohn, W. *Phys. Rev. Lett.* **2001**, *87*, 093001.
(38) (a) Schipper, P. R. T.; Gritsenko, O. V.; Baerends, E.-J. *Theor. Chem. Acc.* **1998**, *99*, 329−343. (b) Schipper, P. R. T.; Gritsenko, O. V.; Baerends, E.-J. *J. Chem. Phys.* **1999**, *111*, 4056−4067.
(39) Morrison, R. C. *J. Chem. Phys.* **2002**, *117*, 10506−10511.
(40) (a) Slater, J. C.; Mann, J. B.; Wilson, T. M.; Wood, J. H. *Phys. Rev.* **1969**, *184*, 672−694. (b) Dunlap, B. I. *Adv. Chem. Phys.* **1987**, *69*, 287−318. (c) Wang, S. G.; Schwarz, W. H. E. *J. Chem. Phys.* **1996**, *105*, 4641−4648.
(41) Filatov, M.; Shaik, S. *Chem. Phys. Lett.* **1999**, *304*, 429−437.
(42) Filatov, M.; Shaik, S. *J. Phys. Chem. A* **2000**, *104*, 6628−6636.
(43) Moreira, I. d. P. R.; Costa, R.; Filatov, M.; Illas, F. *J. Chem. Theory Comput.* **2007**, *3*, 764−774.
(44) Kazaryan, A.; Heuver, J.; Filatov, M. *J. Phys. Chem. A* **2008**, *112*, 12980−12988.
(45) Aquilante, F.; Vico, L. D.; Ferré, N.; Ghigo, G.; Malmqvist, P.-A.; Neogrády, P.; Pedersen, T. B.; Pitonak, M.; Reiher, M.; Roos, B. O.; Serrano-Andrés, L.; Urban, M.; Veryazov, V.; Lindh, R. *J. Comput. Chem.* **2010**, *31*, 224−247.
(46) Frisch, M. J.; Trucks, G. W.; Schlegel, H. B.; Scuseria, G. E.; Robb, M. A.; Cheeseman, J. R.; Scalmani, G.; Barone, V.; Mennucci, B.; Petersson, G. A.; Nakatsuji, H.; Caricato, M.; Li, X.; Hratchian, H. P.; Izmaylov, A. F.; Bloino, J.; Zheng, G.; Sonnenberg, J. L.; Hada, M.; Ehara, M.; Toyota, K.; Fukuda, R.; Hasegawa, J.; Ishida, M.; Nakajima, T.; Honda, Y.; Kitao, O.; Nakai, H.; Vreven, T.; Montgomery, J. A., Jr.; Peralta, J. E.; Ogliaro, F.; Bearpark, M.; Heyd, J. J.; Brothers, E.; Kudin, K. N.; Staroverov, V. N.; Kobayashi, R.; Normand, J.; Raghavachari, K.; Rendell, A.; Burant, J. C.; Iyengar, S. S.; Tomasi, J.; Cossi, M.; Rega, N.; Millam, J. M.; Klene, M.; Knox, J. E.; Cross, J. B.; Bakken, V.; Adamo, C.; Jaramillo, J.; Gomperts, R.; Stratmann, R. E.; Yazyev, O.; Austin, A. J.; Cammi, R.; Pomelli, C.; Ochterski, J. W.; Martin, R. L.; Morokuma, K.; Zakrzewski, V. G.; Voth, G. A.; Salvador, P.; Dannenberg, J. J.; Dapprich, S.; Daniels, A. D.; Farkas, O.; Foresman, J. B.; Ortiz, J. V.; Cioslowski, J.; Fox, D. J. *Gaussian 09*, Revision A.02. 2009; Gaussian Inc.: Wallingford, CT, 2009.
(47) Schmidt, M.; Baldridge, K.; Boatz, J.; Elbert, S.; Gordon, M.; Jensen, J.; Koseki, S.; Matsunaga, N.; Nguyena, K.; Su, S.; Windus, T.; Dupuis, M.; Montgomery, J. *J. Comput. Chem.* **1993**, *14*, 1347−1363.
(48) Gordon, M.; Schmidt, M. In *Theory and Applications of Computational Chemistry, the First Forty Years*; Dykstra, C., Frenking,

G., Kim, K., Scuseria, G., Eds.; Elsevier: Amsterdam, 2005; pp 1167−1189.
(49) Neese, F. *ORCA*, An ab initio, Density Functional and Semiempirical Program Package, Version 2.9.1; Max-Planck Institut for Bioinorganic Chemistry: Muelheim/Ruhr, Germany, 2004.
(50) Giesbertz, K. J. H.; Baerends, E.-J. *J. Chem. Phys.* **2010**, *132*, 194108.
(51) Hirao, K.; Nakatsuji, H. *J. Chem. Phys.* **1973**, *59*, 1457−1462.
(52) Salem, L.; C., R. *Angew. Chem., Int. Ed.* **1972**, *11*, 92−111.
(53) Filatov, M.; Shaik, S. *Chem. Phys. Lett.* **1998**, *288*, 689−697.
(54) Bonačić-Koutecký, V.; Koutecký, J.; Michl, J. *Angew. Chem., Int. Ed.* **1987**, *26*, 170−189.
(55) Filatov, M. unpublished, 2012.
(56) Kraka, E.; Filatov, M.; Zou, W.; Gräfenstein, J.; Izotov, D.; Gauss, J.; He, Y.; Wu, A.; Polo, V.; Olsson, L.; Konkoli, Z.; He, Z.; Cremer, D. *COLOGNE2012*; 2012.
(57) Head-Gordon, M.; Rico, R. J.; Oumi, M.; Lee, T. J. *Chem. Phys. Lett.* **1994**, *219*, 21−29.
(58) Grimme, S.; Neese, F. *J. Chem. Phys.* **2007**, *127*, 154116.
(59) Doltsinis, N. L.; Marx, D. *Phys. Rev. Lett.* **2002**, *88*, 166402.
(60) Bally, T.; Sastry, G. N. *J. Phys. Chem. A* **1997**, *101*, 7923−7925.
(61) Lundberg, M.; Siegbahn, P. E. M. *J. Chem. Phys.* **2005**, *122*, 224103.
(62) Haas, Y.; Gogan, S.; Zilberg, S. *Int. J. Quantum Chem.* **2005**, *102*, 961−970.